

Article

Mann–Kendall-Based Concrete Failure Trend Analysis and Its Implementation for Dynamic Building Monitoring

Xu Yang ^{1,2,3}  and Xueying Han ^{4,*}¹ School of Civil Engineering, Harbin Institute of Technology, Harbin 150090, China² Key Lab of Structures Dynamic Behavior and Control of the Ministry of Education, Harbin Institute of Technology, Harbin 150090, China³ Key Lab of Smart Prevention and Mitigation of Civil Engineering Disasters of the Ministry of Industry and Information Technology, Harbin Institute of Technology, Harbin 150090, China⁴ School of Architecture, Harbin Institute of Technology, Harbin 150006, China

* Correspondence: hanxueyinghxy119@163.com

Abstract: Analyzing monitoring data efficiently is a classic problem in structural health monitoring. A nonparametric test method, the Mann–Kendall (MK) method, was implemented in this study, which is commonly used to detect monotonic trends in a series of environmental data. Using the MK method, three types of time series were studied: the stress time series measured in the concrete prism compression test, the resultant force time series obtained from the pseudostatic test of a reinforced masonry shear wall, and the translation velocity time series detected in a high-rise building. The statistics calculated, as well as the intersections of curves, indicate the trend change in the time series. The results demonstrated that the MK method could efficiently analyze the trend in the engineering time series.

Keywords: trend analysis; monitoring data; Mann–Kendall method; concrete; reinforced masonry



Citation: Yang, X.; Han, X. Mann–Kendall-Based Concrete Failure Trend Analysis and Its Implementation for Dynamic Building Monitoring. *Buildings* **2022**, *12*, 1165. <https://doi.org/10.3390/buildings12081165>

Academic Editor: Fulvio Parisi

Received: 10 July 2022

Accepted: 30 July 2022

Published: 4 August 2022

Publisher's Note: MDPI stays neutral with regard to jurisdictional claims in published maps and institutional affiliations.



Copyright: © 2022 by the authors. Licensee MDPI, Basel, Switzerland. This article is an open access article distributed under the terms and conditions of the Creative Commons Attribution (CC BY) license (<https://creativecommons.org/licenses/by/4.0/>).

1. Introduction

Structural health monitoring could prevent building safety accidents. Efficiently analyzing the monitoring data obtained by varied sensors is a classic problem in structural health monitoring.

The literature in this domain has highlighted several methods. In one class, some of the methods work with threshold analysis theory. For instance, the predefined strain threshold helps to predict the damaged or near-damaged part of modular buildings [1–3]. The residual drift threshold has been introduced to detect the structural reliability of steel frames [4,5]. The ratio Cl-/OH- threshold has been used to assess the concrete corrosion status [6,7]. The fractal dimension has been developed to analyze the aggregates' packing status in concrete [8,9]. Several methods have also been proposed to provide a more accurate dynamically modified threshold value [10]. A prediction framework was introduced to forecast appropriate thresholds using limited data exhibiting nonstationarity to predict the long-term behavior of a concrete dam [11–13]. The Spectral Shift Quality threshold was proposed using distributed optical fiber sensors on the reinforced concrete structures [14]. All the studies reviewed here have a particular problem, in that when a single threshold is exceeded, the construction element or the whole structure is not assumed to be in danger; this may cause a misjudgment.

The second class of research focuses on the statistical or random characteristics of the data measured. A statistical model based on the optimized random forest model was offered to monitor concrete dam deformation [15,16]. The development of long-term structural health monitoring systems for preventive conservation of historic monumental buildings has received a growing trend of scientific interest [17,18]. In addition, random

fields, non-Gaussian stochastic models, and independent component analysis-based arbitrary polynomial chaos methods could offer us an effective framework for stochastic modeling and response propagation of an engineering system [19–22]. Furthermore, several classic machine learning algorithms have been introduced and improved, such as a neural network pattern recognition algorithm to improve pavement maintenance and rehabilitation [23]. These statistical-or-random-characteristics-based analysis methods can process vast amounts of data, which can indicate the structure's status and improve safety. However, these methods usually consume considerable computation time, which limits their development in engineering.

To a certain extent, the structural health monitoring technological progress might be obstructed by the lack of an efficient and accurate monitoring data analysis method. In this study, a trend analysis is introduced based on a nonparametric test method, the Mann–Kendall(MK) method, which is commonly implemented to detect monotonic trends in a series of environmental data [24,25]. It is necessary when applying a parametric test to assume the random distribution of the data series [26]. The nonparametric test method, on the other hand, does not need to consider what random distribution the data samples follow [27]. In addition, the main advantage of the nonparametric test method is that it can be immune to the interference of the abnormal value measured. This advantage makes the MK method applicable to analyze time series efficiently. Three common types of time series were studied, the stress time series measured in the concrete prism compression test, the resultant force time series obtained from the pseudostatic test of a reinforced masonry shear wall, and the translation velocity time series detected in a high-rise building. This study provides a powerful tool for structural health monitoring.

2. Mann–Kendall Method

The MK method was implemented through the following steps:

Step 1. We calculated the statistical sequence of the original time series. First, it was necessary to construct an order list, s_k based on the original time series, x_k , where $k = 1, 2, \dots, n$ indicated the order. The k th item of this order sequence, s_k , was obtained by Equation (1)

$$s_k = \sum_{j=1}^k r_j \quad (1)$$

where element r_j was obtained in the following manner:

$$r_j = \sum_{i=1}^j a_j \quad (2)$$

$$a_j = \begin{cases} 1 & , \text{if } x_j > x_i \\ 0 & , \text{if } x_j \leq x_i \end{cases} \quad i = 1, 2, \dots, j \quad (3)$$

Then, the statistical characteristic values of the series s_k , i.e., the mean value, $E(s_k)$, and variance, $Var(s_k)$, were obtained by the approximation formula Equations (4) and (5), respectively:

$$E(s_k) = \frac{k(k-1)}{4} \quad (4)$$

$$S(s_k) = \frac{k(k-1)(2k+5)}{72} \quad (5)$$

Hence, the statistical sequence UF_k was obtained by applying Equation (6) based on the order list, s_k , and its statistical characteristic values, s_k and $E(s_k)$.

$$UF_k = \frac{s_k - E(s_k)}{\sqrt{Var(s_k)}} \quad (6)$$

Step 2. We calculated the statistical sequence of the reversed time series.

Before calculating the order list, the time series x_1, x_2, \dots, x_n should be reversed; the reversed series was noted as $X' = \{x_n, x_{n-1}, \dots, x_1\}$. The m th element of X' was noted as x'_m .

Then, the cumulative value r'_p was obtained in the following manner:

$$r'_p = \sum_{i=1}^p a_p \quad (7)$$

$$a_p = \begin{cases} 1 & , \text{if } x'_p > x'_i \\ 0 & , \text{if } x'_p \leq x'_i \end{cases} \quad i = 1, 2, \dots, p \quad (8)$$

The m th item of the reversed order sequence, s'_m , was obtained by Equation (9)

$$s'_m = \sum_{p=1}^m r'_p \quad (9)$$

The statistical sequence UF'_m was also obtained by applying Equation (6). By defining $UB_m = -UF'_m$, $m = 1, 2, \dots, n$, the statistical sequence of reversed time series was obtained.

Step 3. We analyzed the trend according to the order list of the time series and its reversed series.

The analysis started with plotting the statistical sequence of UF_k and UB_m . According to the sequence of the UF and UB values, the following analyses were made:

1. The UF value larger than 0 or the UB value smaller than 0 indicated an increasing trend. Conversely, the negative value of UF indicated a decreasing trend.
2. The UF or UB value exceeding the threshold demonstrated a remarkable trend, which was considered an abrupt and sudden change.
3. The intersection of the curves of UF and UB indicate a possible significance in the change.

In addition, the sequence of UF followed the standard normal distribution. With the statistical significance level, α , given, the UF_k larger than the $(1 - \alpha/2)$ th percentile of the standard normal distribution indicated a remarkable change trend.

3. Experiments

3.1. Concrete Prism under Axial Compression

The first type of testing sample analyzed in this study was a concrete prism with dimensions of 150 mm \times 150 mm \times 300 mm (length \times width \times height) under axial compression, as shown in Figure 1. The coarse aggregate content was 50%. The other components' content of this sample was as follows: 195 kg/m³ of water, 325 kg/m³ of cement, and 696 kg/m³ of sand.

Then, the concrete prism sample was tested with a closed-loop servo-controlled compression testing machine with a capacity of 200 kN. The compressive load was applied in displacement-control mode. The sample's load and deformation were measured by a pressure sensor and linear variable differential transformer (LVDT).

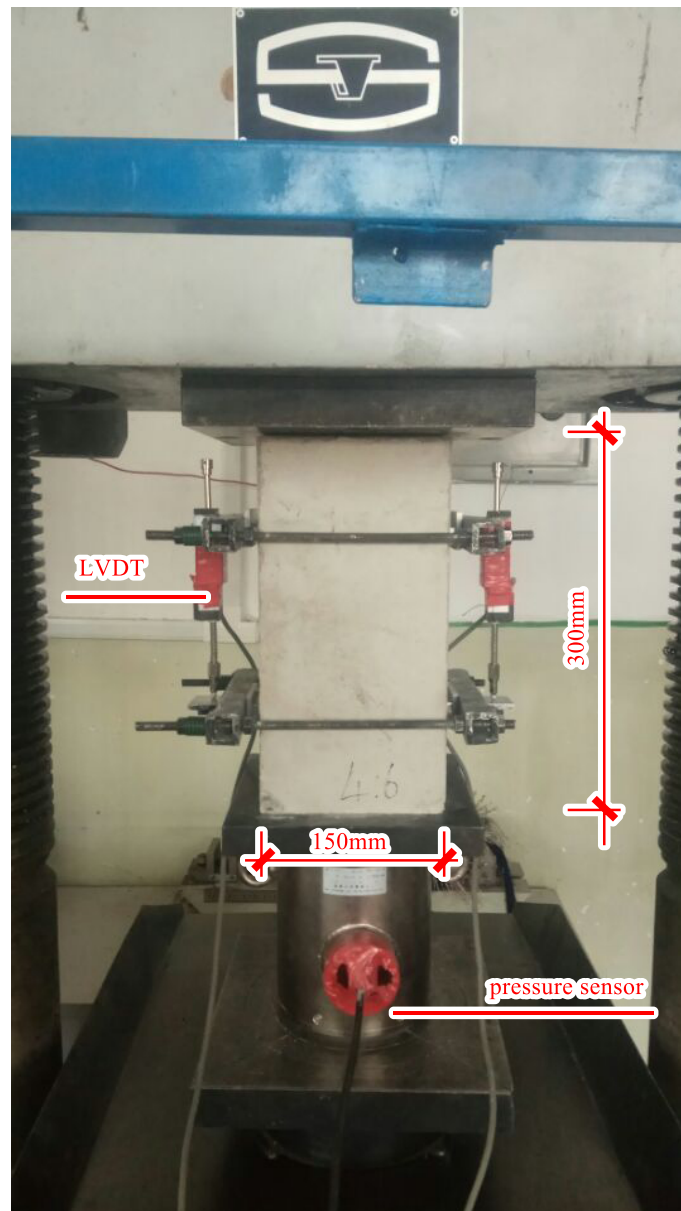


Figure 1. Concrete prism compression test.

3.2. Reinforced Masonry Shear Wall under Lateral Cyclic Load

The second case studied was a reinforced masonry shear wall under lateral cyclic load. The sample had a high aspect ratio with dimensions of 1390 mm × 3200 mm × 190 mm (length × height × thickness). This shear wall was constructed by using hollow concrete blocks with an average compressive strength of 22.8 MPa, mortar with an average compressive strength of 21.5 MPa, grouted concrete with an average compressive strength of 32.2 MPa, a horizontal steel bar with an average yield strength of 393 MPa, and a vertical steel bar with an average yield strength of 405 MPa. The detailed setup of the cyclic loading test can be found in Section 2 of Ref. [28].

Then, a cyclic lateral load was imposed on the wall by displacement-control mode. The loading scheme was illustrated in Figure 7, Section 2 of Ref. [28]. More details about the sample as well as its components and the experiment can be found in our previous study [28].

3.3. Dynamic Building Monitoring

The third analysis object was a translation velocity time series detected in a high-rise building. This building had a height of 99.8 m, constructed by a reinforced concrete hollow block masonry structure. The time series were detected by an accelerometer and data acquisition system set on the 10th floor under the ambient excitation of the building's construction. The accelerometer was installed in the middle of the floor, because this location had a larger stiffness. The detailed schematic diagram of the sensor layout was reported in Section 6 of Ref. [29]. More details about the building, detecting system, and scheme can be found in Ref. [29].

4. Results and Discussion

4.1. Concrete Prism under Axial Compression

The mechanical test and setup were introduced in Section 3.1. Since the load was controlled by displacement, the stress of the prism sample calculated based on the data measured from the pressure sensor is analyzed and discussed. The trend analysis results, i.e., the curves of UF and UB , as well as the original stress time series are plotted in Figure 2.

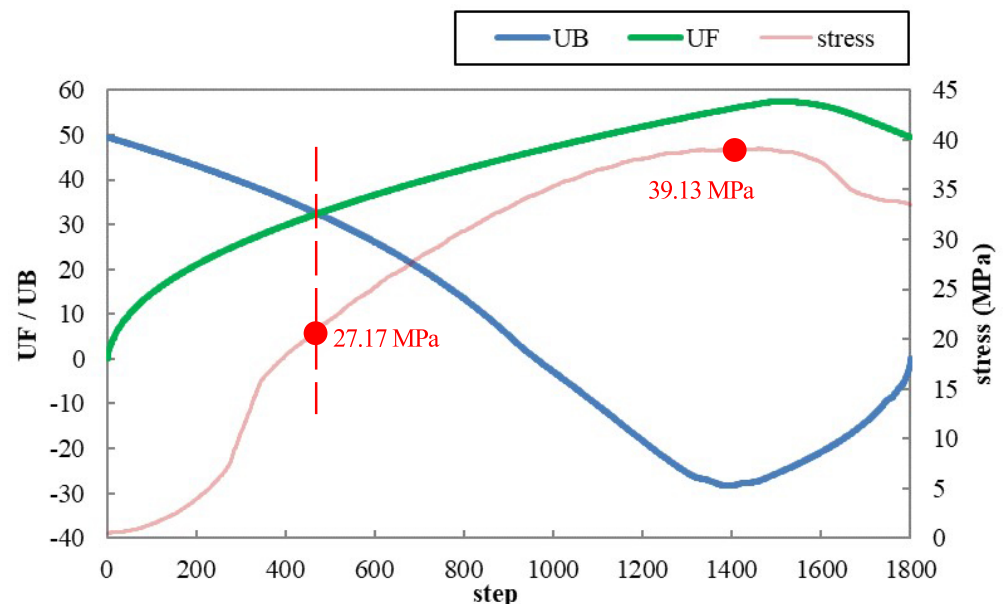


Figure 2. Trend analysis of stress time series measured by concrete prism under axial compression.

The stress time series obtained essentially represented the concrete sample's mechanical response under monotonic loading. According to the analysis results represented in Figure 2, the following aspects can be highlighted:

At the very beginning of the loading stage, the UF value was already much larger than 0, which indicated a remarkably increasing trend. This phenomenon might be caused directly by the monotonic loading mode. The gradually increased compressive load increased stress, as well as the development of eventual failure. That is to say, in the case that the concrete prism sample was subjected to a monotonic compressive loading, the stress trend would increase. The monotonic compressive loading would cause the sample's inevitable failure.

Next, the time of the abrupt and sudden change occurrence is discussed. As mentioned above, the UF or UB value exceeding the threshold demonstrated a remarkable trend, which could be considered an abrupt and sudden change. The UF value exceeded the threshold $\Phi(\alpha = 0.1) = \pm 1.96$ at the very beginning of the loading stage, which also demonstrated that a monotonic gradually increasing compressive loading would cause the sample's inevitable failure. Meanwhile, the intersection of the curves of UF and UB was located in the elastic stage, when the stress reached about 21 MPa. This intersection

location indicated that the possible significance of the change occurred when the stress reached about 50% of the compressive strength, 39 MPa. In other words, if the concrete prism sample was subjected to a monotonic compressive loading, the possible significance of stress change might take place when about 50% of the maximum load was imposed.

4.2. Reinforced Masonry Shear Wall under Lateral Cyclic Load

The pseudostatic test and setup were introduced in Section 3.2. Since the load imposed on the shear wall was controlled displacement, the resultant force of the shear wall sample is analyzed and discussed. The trend analysis results, as well as the original resultant force time series, are plotted in Figure 3.

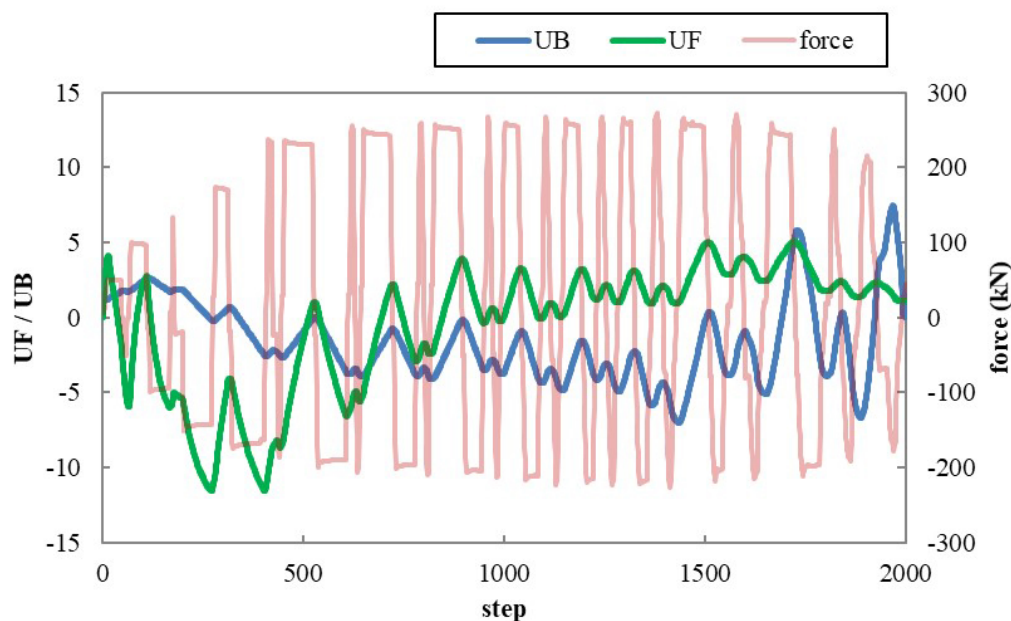


Figure 3. Trend analysis of resultant force time series measured by reinforced masonry shear wall under lateral cyclic load.

The resultant force series obtained essentially represented the reinforced concrete block masonry shear wall's mechanical response under cyclic loading. According to the analysis results represented in Figure 3, the following aspects can be highlighted:

At the beginning of the loading stage, i.e., when the amplitude of displacement gradually increased and plastic deformation was not produced in the steel bar, the UF value declined with a significant fluctuation. This negative sequence of UF indicated an obvious decreasing trend. Meanwhile, the fluctuation could be considered to be caused by the cyclic loading mode. This observation can be explained by the reinforced masonry structure's mechanical characteristics. This type of structure had adequate safety storage in its early loading stage when the steel retained elastic. This phenomenon demonstrated that the reinforced masonry shear wall would not suffer from unexpected brittle fracturing as long as the reinforcement did not begin to yield.

As the lateral displacement imposed on the shear wall grew, the UF increased from the basement with fluctuations. This increase in the UF value was considered as a mark of the steel bar entering plastic deformation. When the UF increased with fluctuation, the first intersection of the curves of UF and UB occurred, which could indicate a possible significance in the change that might appear in the cyclic loading stage. Then, more intersections were observed during the cyclic loading stage; each intersection location indicated a possible sudden trend change. At that moment, a new crack or a remarkable propagation of crack might be observed. However, because of the cyclic loading mode, this new crack (or expanded crack) closed under the load imposed in the opposite direction. Meanwhile, the trend change became stable again. This process would continue until the

failure of the steel bar. This phenomenon also demonstrated the adequate safety storage of the reinforced masonry shear wall in its plastic phase.

4.3. Building Dynamic Monitoring

The first and second series discussed above were more likely obtained from a sample subjected to the load following a certain strategy, the third sampling process was more random. The trend analysis results, as well as the original translation velocity time series, are plotted in Figure 4.

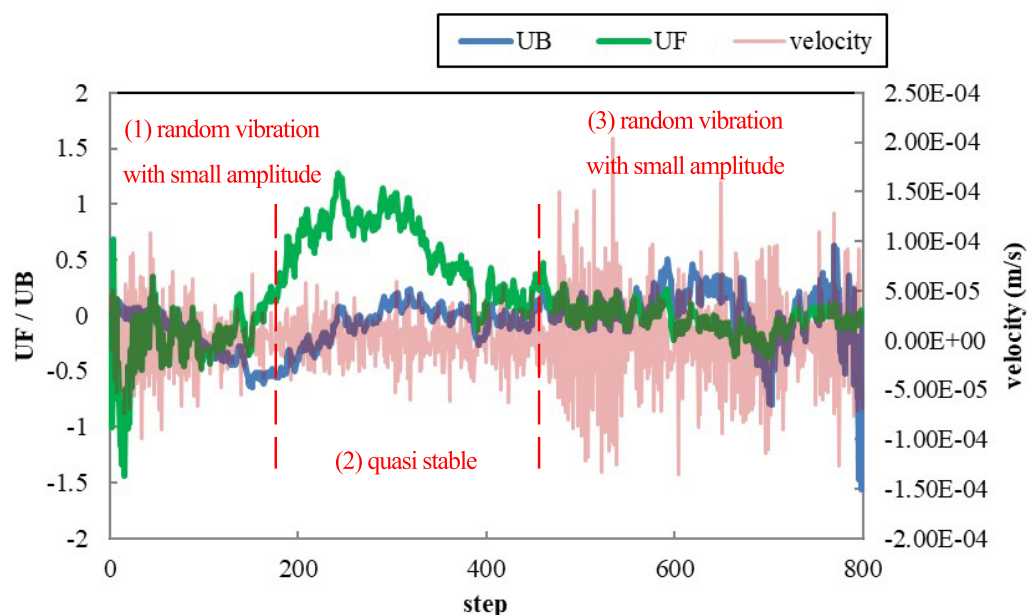


Figure 4. Trend analysis of translation velocity time series measured in a high-rise building.

According to Figure 4, this time series was divided into three parts: (1) the random vibrations with low amplitude from the 0 to 200th step, (2) the quasi-stable phase from the 200th to 400th step, and (3) the random vibration with higher amplitude from the 400th to 800th step.

The UF curve fluctuated severely in the first part with the translation velocity values fluctuating. Meanwhile, the segment of the UF curve in the second part, the quasi-stable part, represented a remarkable increase. This phenomenon might be explained by the manner of intercepting the curve. The selected time series started with a fluctuation, and the quasi-stable part would have an obvious different vibration characteristic from the former part. This shift in the vibration characteristics caused the change in the statistical parameters. Then, the UF curve fluctuated when the vibration characteristics altered. Therefore, it should be noticed that the manner of intercepting random vibration time series influenced the UF curve. Although the MK method was successfully developed and applied in analyzing the random time series [30], several researchers have mentioned that a high sampling frequency or large sample number might cause a misjudgment [31]. In addition, the analysis results obtained based on the MK method can only provide the statistical trend change, the physical significance of the trend change needs to be determined based on other mathematical models [27]. That is to say, the value of UF might not be applicable to analyze the trend of the object under a random vibration with a high sampling frequency.

On the other hand, the intersections of the curves of UF and UB were commonly observed near the dividing boundary of the parts mentioned above, which indicated that a possible sign of change appeared when the amplitude changed considerably. In other words, both the intersections of the curves of UF and UB analysis and monitoring of the change of amplitude might be efficient to determine a sudden change under a random vibration.

5. Conclusions and Future Works

5.1. Conclusions

This study analyzed three types of time series, the stress time series measured in the concrete prism compression test, the resultant force time series obtained from the pseudostatic test of a reinforced masonry shear wall, and the translation velocity time series detected in a high-rise building, based on the Mann–Kendall (MK) method. The following conclusions can be drawn:

1. A UF value larger than 0 at the beginning of the loading stage of the concrete prism compression test indicated the monotonic compressive loading would cause the sample's inevitable failure. The location of the intersection of the curves of UF and UB indicated that the possible significance of a stress change might take place when about 50% of the maximum load was imposed.
2. The fluctuation of the UF curve obtained according to the resultant force time series analysis demonstrated that the reinforced masonry shear wall would not suffer from unexpected brittle fracturing as long as the reinforcement did not start yielding. Furthermore, the adequate safety storage in its plastic phase was shown.
3. The value of UF might not be applicable to analyze the trend of an object under a random vibration with a high sampling frequency. However, both the intersections of the curves of UF and UB analysis and monitoring the change in amplitude might be efficient to determine the sudden change under a random vibration.

This study demonstrated that the MK method could be efficient in analyzing the trend in engineering time series. The analysis results can indicate and predict the sudden change in the trend, which provides a powerful tool for structural health monitoring.

5.2. Future Work

As a nonparametric test method, the MK method has an intrinsic limitation. This method can only provide the statistical trend change; the physical significance of the trend change needs to be determined based on other mathematical models. We will attempt to overcome these disadvantages in our future work.

Author Contributions: Conceptualization, X.H.; Funding acquisition, X.H.; Software, X.Y.; Writing—original draft, X.Y.; Writing—review and editing, X.H. All authors have read and agreed to the published version of the manuscript.

Funding: This work was supported by the China Postdoctoral Science Foundation Grant (No. 2019M651292 and No. 2019T120273), the National Natural Science Foundation of China (No. 52008135), and the Province Heilongjiang Postdoctoral Science Foundation Grant (No. LBH-Z20010).

Institutional Review Board Statement: Not applicable.

Informed Consent Statement: Not applicable.

Data Availability Statement: Not applicable.

Conflicts of Interest: The authors declare no conflict of interest.

References

1. Sivasuriyan, A.; Vijayan, D.S.; Górski, W.; Wodzyński, Ł.; Vaverková, M.D.; Koda, E. Practical implementation of structural health monitoring in multi-story buildings. *Buildings* **2021**, *11*, 263. [\[CrossRef\]](#)
2. Valinejadshoubi, M.; Bagchi, A.; Moselhi, O. Development of a BIM-based data management system for structural health monitoring with application to modular buildings: Case study. *J. Comput. Civ. Eng.* **2019**, *33*, 05019003. [\[CrossRef\]](#)
3. Mannino, A.; Dejaco, M.C.; Re Cecconi, F. Building information modelling and internet of things integration for facility management—Literature review and future needs. *Appl. Sci.* **2021**, *11*, 3062. [\[CrossRef\]](#)
4. Bojórquez, E.; López-Barraza, A.; Reyes-Salazar, A.; Ruiz, S.E.; Ruiz-García, J.; Formisano, A.; López-Almansa, F.; Carrillo, J.; Bojórquez, J. Improving the structural reliability of steel frames using posttensioned connections. *Adv. Civ. Eng.* **2019**, *2019*. [\[CrossRef\]](#)
5. Montuori, R.; Nastri, E.; Todisco, P. Influence of the seismic shear proportioning factor on steel MRFs seismic performances. *Soil Dyn. Earthq. Eng.* **2021**, *141*, 106498. [\[CrossRef\]](#)

6. Rodrigues, R.; Gaboreau, S.; Gance, J.; Ignatiadis, I.; Betelu, S. Reinforced concrete structures: A review of corrosion mechanisms and advances in electrical methods for corrosion monitoring. *Constr. Build. Mater.* **2021**, *269*, 121240. [[CrossRef](#)]
7. Femenias, Y.S.; Angst, U.; Moro, F.; Elsener, B. Development of a novel methodology to assess the corrosion threshold in concrete based on simultaneous monitoring of pH and free chloride concentration. *Sensors* **2018**, *18*, 3101. [[CrossRef](#)]
8. Wang, M.; Yang, X.; Wang, W. Establishing a 3D aggregates database from X-ray CT scans of bulk concrete. *Constr. Build. Mater.* **2022**, *315*, 125740. [[CrossRef](#)]
9. Yang, X.; Wang, F.; Yang, X.; Zhou, Q. Fractal dimension in concrete and implementation for meso-simulation. *Constr. Build. Mater.* **2017**, *143*, 464–472. [[CrossRef](#)]
10. Dai, H.; Zhang, H.; Rasmussen, K.J.; Wang, W. Wavelet density-based adaptive importance sampling method. *Struct. Saf.* **2015**, *52*, 161–169. [[CrossRef](#)]
11. Prakash, G.; Sadhu, A.; Narasimhan, S.; Brehe, J.M. Initial service life data towards structural health monitoring of a concrete arch dam. *Struct. Control Health Monit.* **2018**, *25*, e2036. [[CrossRef](#)]
12. Ren, Q.; Li, M.; Li, H.; Song, L.; Si, W.; Liu, H. A robust prediction model for displacement of concrete dams subjected to irregular water-level fluctuations. *Comput.-Aided Civ. Infrastruct. Eng.* **2021**, *36*, 577–601. [[CrossRef](#)]
13. Wang, S.; Xu, C.; Liu, Y.; Wu, B. Mixed-coefficient panel model for evaluating the overall deformation behavior of high arch dams using the spatial clustering. *Struct. Control Health Monit.* **2021**, *28*, e2809. [[CrossRef](#)]
14. Barrias, A.; R. Casas, J.; Villalba, S. Embedded distributed optical fiber sensors in reinforced concrete structures—A case study. *Sensors* **2018**, *18*, 980. [[CrossRef](#)] [[PubMed](#)]
15. Dai, B.; Gu, C.; Zhao, E.; Qin, X. Statistical model optimized random forest regression model for concrete dam deformation monitoring. *Struct. Control Health Monit.* **2018**, *25*, e2170. [[CrossRef](#)]
16. Pan, Y.; Zhang, L. Roles of artificial intelligence in construction engineering and management: A critical review and future trends. *Autom. Constr.* **2021**, *122*, 103517. [[CrossRef](#)]
17. Kita, A.; Cavalagli, N.; Ubertini, F. Temperature effects on static and dynamic behavior of Consoli Palace in Gubbio, Italy. *Mech. Syst. Signal Process.* **2019**, *120*, 180–202. [[CrossRef](#)]
18. Han, Q.; Ma, Q.; Xu, J.; Liu, M. Structural health monitoring research under varying temperature condition: A review. *J. Civ. Struct. Health Monit.* **2021**, *11*, 149–173. [[CrossRef](#)]
19. Zhang, R.; Dai, H. Independent component analysis-based arbitrary polynomial chaos method for stochastic analysis of structures under limited observations. *Mech. Syst. Signal Process.* **2022**, *173*, 109026. [[CrossRef](#)]
20. Dai, H.; Zhang, R.; Beer, M. A new perspective on the simulation of cross-correlated random fields. *Struct. Saf.* **2022**, *96*, 102201. [[CrossRef](#)]
21. Zhang, R.; Dai, H. A non-Gaussian stochastic model from limited observations using polynomial chaos and fractional moments. *Reliab. Eng. Syst. Saf.* **2022**, *221*, 108323. [[CrossRef](#)]
22. Zheng, Z.; Dai, H. A new fractional equivalent linearization method for nonlinear stochastic dynamic analysis. *Nonlinear Dyn.* **2018**, *91*, 1075–1084. [[CrossRef](#)]
23. Elbagalati, O.; Elseifi, M.A.; Gaspard, K.; Zhang, Z. Development of an enhanced decision-making tool for pavement management using a neural network pattern-recognition algorithm. *J. Transp. Eng. Part B Pavements* **2018**, *144*, 04018018. [[CrossRef](#)]
24. Gocic, M.; Trajkovic, S. Analysis of changes in meteorological variables using Mann–Kendall and Sen’s slope estimator statistical tests in Serbia. *Glob. Planet. Chang.* **2013**, *100*, 172–182. [[CrossRef](#)]
25. Mallick, J.; Talukdar, S.; Alsubih, M.; Salam, R.; Ahmed, M.; Kahla, N.B.; Shamimuzzaman, M. Analysing the trend of rainfall in Asir region of Saudi Arabia using the family of Mann–Kendall tests, innovative trend analysis, and detrended fluctuation analysis. *Theor. Appl. Climatol.* **2021**, *143*, 823–841. [[CrossRef](#)]
26. Pohlert, T. Non-Parametric Trend Tests and Change-Point Detection. 2016. Available online: <https://mran.microsoft.com/snapshot/2016-06-30/web/packages/trend/vignettes/trend.pdf> (accessed on 8 July 2022).
27. Garrido-Martín, D.; Calvo, M.; Reverter, F.; Guigó, R. A fast non-parametric test of association for multiple traits. *bioRxiv* **2022**. [[CrossRef](#)]
28. Xu, W.; Yang, X.; Wang, F. Experimental investigation on the seismic behavior of newly-developed precast reinforced concrete block masonry shear walls. *Appl. Sci.* **2018**, *8*, 1071. [[CrossRef](#)]
29. Yan, Z. Research on Seismic Behavior and Dynamic Testing of 100-Meter Reinforced-Block Masonry Shear Wall Structures. PhD Thesis, Harbin Institute of Technology, Harbin, China, 2015.
30. Kedem, B.; Fokianos, K. *Regression Models for Time Series Analysis*; John Wiley & Sons: Hoboken, NJ, USA, 2005.
31. Yue, S.; Wang, C.Y. Applicability of prewhitening to eliminate the influence of serial correlation on the Mann–Kendall test. *Water Resour. Res.* **2002**, *38*, 4-1–4-7. [[CrossRef](#)]